Journal of Physics: Conference Series **774** (2016) 012094 doi:10.1088/1742-6596/774/1/012094

The CABARET method for a weakly compressible fluid flows in one- and two-dimensional implementations

Yu M Kulikov and E E Son

Joint Institute for High Temperatures of the Russian Academy of Sciences, Izhorskaya 13 Bldg 2, Moscow 125412, Russia

E-mail: kulikov-yurii@yandex.ru

Abstract. The CABARET method implementation for a weakly compressible fluid flow is in the focus of present paper. Testing both one-dimensional pressure balancing problem and a classical plane Poiseuille flow, we analyze this method in terms of discontinuity resolution, dispersion and dissipation. The method is proved to have an adequate convergence to an analytical solution for a velocity profile. We also show that a flow formation process represents a set of self-similar solutions under varying pressure differential and sound speed.

1. Introduction

Numerical simulations being an inalienable part of hydrodynamical studies can either possess an inherent value when solving classical problems of computational fluid dynamics (CFD) and testing new mathematical methods or support experimental investigations providing optimal parameters for laboratory facilities. Despite computational power constant increase the actual efficiency of CFD algorithms crucially depends on numerical scheme chosen and the scale of parallelism. It were Samarskii and Goloviznin [1] which gave rise to the novel numerical scheme (the CABARET method) representing a new approach to simulate fluid flows dominated by convective transfer including shock-wave propagation, aeroacoustics, vortex and turbulent flows and thermal convection. The CABARET method [2] is based on a single-cell space-time pattern providing formally second-order flow approximations unless nonlinear correction procedure is required. The nonlinear correction algorithm employs the maximum principle for local Riemann invariants to suppress oscillations efficiently. The CABARET numerical scheme solves governing equations explicitly both for strong shock and weak acoustic waves without any fudge factors and does not need any iterative procedures. Its remarkable properties are conditioned by a superset of variables, that includes the so-called "flux-type variables" (related to the centers of cell facets) along with the usual "conservative" variables and in some cases causes 4-fold increase of computer memory size requirements.

The approach considered further provides a competitive alternative [3] to well-known second-order total variation diminishing (TVD) schemes (such as Roe upwind scheme with Van Leer's, MinMod, SuperBee or Tishkin's [4] upwind biased limiters) when resolving shock waves and expansion fans in the one-dimensional gasdynamic problems. Studying the evolution of the sinusoidal velocity profile [2] in a wide range of Courant numbers showed that the CABARET

scheme does not generate any unphysical discontinuities in a smooth profile, unlike standard TVD (SuperBee, MinMod and Tishkin's) methods.

The present paper is focused on the CABARET scheme testing for the weakly compressible fluid to confirm its features claimed by the developers.

2. One-dimensional formulation

There are several different implementations of the CABARET method developed for gasdynamic flows, incompressible fluids in which the equations are solved in pressure–velocity [5] or vorticity–stream function [6] formulations. Besides that, the number of invariants transferred over the mesh differs. Actually, weakly compressible fluid model falls in between foregoing ones, allowing to simplify local invariants selection algorithm and also to avoid solving Laplace equation for pressure.

2.1. General algorithm discussion

This section provides a detailed description of the CABARET algorithm for one-dimensional problems, as well as for the isothermal plane viscous fluid flow. Our further treatment is intended to reduce the number of disambiguations associated with the algorithm implementation, as also to draw an attention to some interesting aspects.

Let us write the homogeneous equations in the divergent form corresponding to continuity and momentum equations in a one-dimensional formulation:

$$\frac{\partial \rho}{\partial t} + \frac{\partial \rho u}{\partial x} = 0, \tag{1}$$

$$\frac{\partial \rho u}{\partial t} + \frac{\partial \rho u^2}{\partial x} + \frac{\partial p}{\partial x} = 0, \tag{2}$$

complemented by the barotropic equation of state for weakly compressible fluid

$$p = c^2(\rho - \rho_0), \quad \frac{\mathrm{d}\rho}{\mathrm{d}p} = \frac{1}{c^2}. \tag{3}$$

One can reformulate the above equations so that the k-th equation will contain directional derivatives in the plane (x, t) of the form

$$\frac{\partial}{\partial t} + \lambda_k \frac{\partial}{\partial x}. \tag{4}$$

If such a conversion is possible for simultaneous linear and quasi-linear equations and the determinant of coefficients matrix at derivatives (4) is nonzero, they are called hyperbolic [7]:

$$\vec{\phi}^T = (\rho, u, v), \tag{5}$$

$$\frac{\partial \vec{\phi}}{\partial t} + A_x \frac{\partial \vec{\phi}}{\partial x} = 0, \tag{6}$$

$$\frac{\partial \rho}{\partial t} + u\frac{\partial \rho}{\partial x} + c^2 \rho \frac{\partial u}{\partial x} = 0, \tag{7}$$

$$\frac{\partial u}{\partial t} + u\frac{\partial u}{\partial x} + \frac{1}{\rho}\frac{\partial p}{\partial x} = 0, \tag{8}$$

$$A_x = \begin{pmatrix} u & c^2\rho \\ 1/\rho & u \end{pmatrix}. \tag{9}$$

Eigenvalues of A_x are different real numbers:

$$\lambda_1^x = u + c, \quad \lambda_2^x = u - c, \tag{10}$$

so that A_x satisfies an alternative definition [2] of hyperbolic system. The transposed eigenvectors matrix have the following form:

$$\Omega_x = \begin{pmatrix} 1/\rho c & 1 \\ -1\rho c & 1 \end{pmatrix}. \tag{11}$$

Thus, homogeneous simultaneous equations are shaped into:

$$\frac{\partial I_k^x}{\partial t} + \lambda_k^x \frac{\partial I_k^x}{\partial x} = 0, \quad k = 1, 2, \tag{12}$$

where I_k^x denotes Riemann invariants:

$$I_1^x = u + c\ln(p(\rho) + c^2\rho_0), \quad I_2^x = u - c\ln(p(\rho) + c^2\rho_0). \tag{13}$$

At this point one can raise a question if it's possible to use Taylor series expansion in (13) due to the obvious relation between terms $c^2\rho_0 >> |p|$ in a real fluid. Such a transformation proposed in the original monograph yields

$$I_1^x = u + \frac{p}{c^2\rho_0}, \quad I_1^x = u - \frac{p}{c^2\rho_0}. \tag{14}$$

In fact, this operation can conceal an uncertain risk when an automatic selection of the sound speed is used to maintain current step Mach number being $M \leq 0.1$.

Hereafter the index i denotes the points in X direction, whereas n numerates time layers, $i + 1/2$ is referred to flux-type variables, $n + 1/2$ relates only to the conservative variables of the intermediate time layer.

To determine conservative variables at a new time layer one need to perform following main stages:

(i) an initialisation of conservative variables at internal points of the computational domain and flux-type variables at the edges with respect to boundary conditions, followed by the interpolation of adjacent flux variables;

(ii) time step calculation grounded stability condition for explicit method

$$\tau = \mathrm{CFL}\Delta x \max(|\lambda_1^x|, |\lambda_2^x|),$$

where $\mathrm{CFL} = 0.15 < 1$ denotes Courant number;

(iii) conservative variable calculation at the intermediate $(n + 1/2)$-layer utilising homogeneous equations

$$\frac{[\mathbb{R}]_{i+\frac{1}{2}}^{n+\frac{1}{2}} - [\mathbb{R}]_{i+\frac{1}{2}}^{n}}{\tau_{n+\frac{1}{2}}/2} + \frac{[\rho u]_{i+1}^n - [\rho u]_i^n}{\Delta x_{i+\frac{1}{2}}} = 0, \tag{15}$$

$$\frac{[\mathbb{R}U]_{i+\frac{1}{2}}^{n+\frac{1}{2}} - [\mathbb{R}U]_{i+\frac{1}{2}}^{n}}{\tau_{n+\frac{1}{2}}/2} + \frac{[\rho u^2 + p]_{i+1}^n - [\rho u^2 + p]_i^n}{\Delta x_{i+\frac{1}{2}}} = 0. \tag{16}$$

(iv) Next one should calculate first two invariants transported through the cell in the X-direction basing known n-layer flux-type variables and $(n-1/2)$-layer conservative variables:

$$\begin{array}{ll} [I_x^1]_i^n = c\ln([p]_i^n + c^2\rho_0) + [u]_i^n, & [I_x^1]_i^n = -c\ln([p]_i^n + c^2\rho_0) + [u]_i^n, \\ [I_x^1]_i^{n+\frac{1}{2}} = c\ln([p]_i^{n+\frac{1}{2}} + c^2\rho_0) + [u]_i^{n+\frac{1}{2}}, & [I_x^2]_i^{n+\frac{1}{2}} = -c\ln([p]_i^{n+\frac{1}{2}} + c^2\rho_0) + [u]_i^{n+\frac{1}{2}}. \end{array} \tag{17}$$

After that we extrapolate these invariants to $(n+1)$-transient layer:

$$\lambda_1^x = u + c > 0, \quad [I_1^x]_i^{n+1} = 2[I_1^x]_{i-\frac{1}{2}}^{n+\frac{1}{2}} - [I_1^x]_{i-1}^n, \tag{18}$$

$$\lambda_2^x = u - c < 0, \quad [I_2^x]_i^{n+1} = 2[I_2^x]_{i+\frac{1}{2}}^{n+\frac{1}{2}} - [I_2^x]_{i+1}^n, \tag{19}$$

and correct them according to the maximum principle:

$$[I_l^x]_i^{n+1} = \begin{cases} [I_l^x]_i^{n+1}, & \text{if } \min(I_l^x) \le [I_l^x]_i^{n+1} \le \max(I_l^x) \\ \min(I_l^x), & \text{if } [I_l^x]_i^{n+1} < \min(I_l^x) \\ \max(I_l^x), & \text{if } [I_l^x]_i^{n+1} > \max(I_l^x) \end{cases}, \quad l = 1, 2, \tag{20}$$

where

$$\max(I_1^x) = \max\left\{[I_1^x]_{i-1}^n, [I_l^x]_{i-\frac{1}{2}}^n, [I_l^x]_i^n\right\}, \quad \min(I_1^x) = \min\left\{[I_1^x]_{i-1}^n, [I_1^x]_{i-\frac{1}{2}}^n, [I_l^x]_i^n\right\}, \tag{21}$$

$$\max(I_2^x) = \max\left\{[I_2^x]_{i+1}^n, [I_1^x]_{i+\frac{1}{2}}^n, [I_1^x]_i^n\right\}, \quad \min(I_2^x) = \min\left\{[I_2^x]_{i+1}^n, [I_2^x]_{i+\frac{1}{2}}^n, [I_2^x]_i^n\right\}. \tag{22}$$

(v) The invariants found yield flux variables $[u]_i^{n+1}$,$[p]_i^{n+1}$ on the new time layer:

$$[u]_i^{n+1} = \frac{I_1^x + I_2^x}{2}, \quad [p]_i^{n+1} = -c^2\rho_0 + \mathrm{e}^{(I_1^x - [u]_i^{n+1})/c}, \quad [\rho]_i^{n+1} = \rho([p]_i^{n+1}). \tag{23}$$

(vi) Finally we move to new conservative variables on the $(n+1)$-layer utilising second-order accuracy finite-difference equations (FDE):

$$\frac{[\mathbb{R}]_{i+\frac{1}{2}}^{n+1} - [\mathbb{R}]_{i+\frac{1}{2}}^n}{\tau_{n+\frac{1}{2}}/2} + \frac{[\overline{\rho u}]_{i+1} - [\overline{\rho u}]_i}{\Delta x_{i+\frac{1}{2}}} = 0, \tag{24}$$

$$\frac{[\mathbb{R}U]_{i+\frac{1}{2}}^{n+1} - [\mathbb{R}U]_{i+\frac{1}{2}}^n}{\tau_{n+\frac{1}{2}}/2} + \frac{[\overline{\rho u^2 + p}]_{i+1} - [\overline{\rho u^2 + p}]_i}{\Delta x_{n+\frac{1}{2}}} = 0. \tag{25}$$

The overline denotes flux-type variables averaged over time layers n and $n+1$.

2.2. Program implementation

The algorithm was implemented in sequential and parallel versions in Fortran 90. Since we used shared memory system, OpenMP parallel technology was employed. The following parameters were set in the original data file: sound speed $c = 1500.0$ m/s, computational domain size $L_X = 2.0$ m, initial velocity $U_{\text{init}} = 0.0$ m/s, initial pressure $P_{\text{init}} = 101325.0$ Pa, velocity boundary condition $U_{\text{inlet}} = 0.0$ m/s, pressure boundary condition $P_{\text{inlet}} = 1013250.0$ Pa. Courant number CFL = 0.15. We solved the problem of pressure equalisation [7] dividing computational domain in two parts and setting the left-side pressure tenfold higher compared to

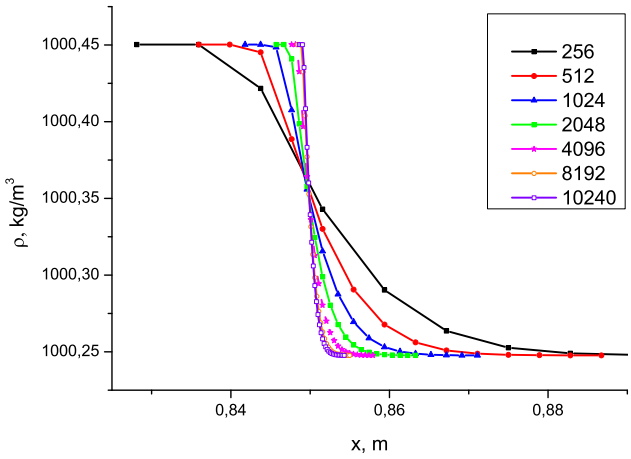

Figure 1. Spatial distribution of density in a pressure gradient zone at $t = 2\times10^{-4}$ s. Numerals in explanatory legend correspond to various number of points n_X in domain.

the right-side one. At the boundary points we set conditions relevant to free fluid outflow. One can estimate acoustic wave propagation time t, time step size τ and total number time steps nT:

$$t = L_X/c \approx 1.3 \times 10^{-3} \text{ s}, \quad \Delta x = L_X/n_X \approx 1.953 \times 10^{-4} \text{ m}, \tag{26}$$

$$\tau = 0.1\Delta x/c \approx 1.302 \times 10^{-8} \text{ s}, \qquad n_T = n_X/CFL = 102400. \tag{27}$$

The grid convergence tests were carried out for various number of grid points in the range of $n_X = 256, \ldots, 10240$, showing the pressure wave steepening as well as the absence of any oscillations which were damped by the nonlinear correction algorithm. However, developers' claim that the shock wave "spreads" on a single cell seems to be unconfirmed, the mesh refinement leads to the spatial gradient wave broadening while increasing the number of points of the gradient zone (see figure 1). The pressure equalising process is limited by sound speed and accompanied by the perturbed fluid flow to the lower density region. The absence of a developed rarefaction wave traveling to the left is another feature. The flat-topped velocity graph expanding to the borders of the computational domain is not presented here because of its triviality.

We used one-dimensional problem of pressure equalization for parallel efficiency testing measuring average execution time of 4 parallel sections—per one for each of computational procedures. This time was calculated using OpenMP library built-in function *omp_get_wtime*() and averaged with respect to all time cycles executed. The total number of points calculated was $n_X = 10240$. Maximum performance was achieved when the number of execution threads (*num_threads*) corresponds to the number of physical processor cores. Further increase of *num_threads* leads to rather sharp performance drop.

2.3. Compression wave running up from the left border

The initial values of conservative variables of the density $\mathbb{R}$ and the velocity U are given by $\mathbb{R} = 1000.0$ kg/m^3, $U = 0.0$ m/s. A compression wave parameters at the left boundary are determined by invariant I_1^x based on the far-field flow pressure $p = P_{\text{inlet}} = 10P_{\text{init}}$ and velocity $u = U_{\text{inlet}} = 0.0$ m/s and invariant I_2^x coming from the interior points of the domain. At the

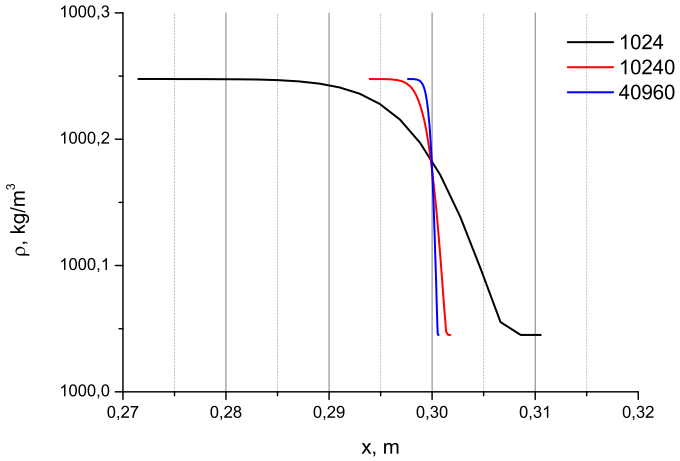

Figure 2. Pressure gradient zone in a (ρ, x) plane at $t = 2.0 \times 10^{-4}$ s. Numerals in explanatory legend correspond to various number of computational points n_X.

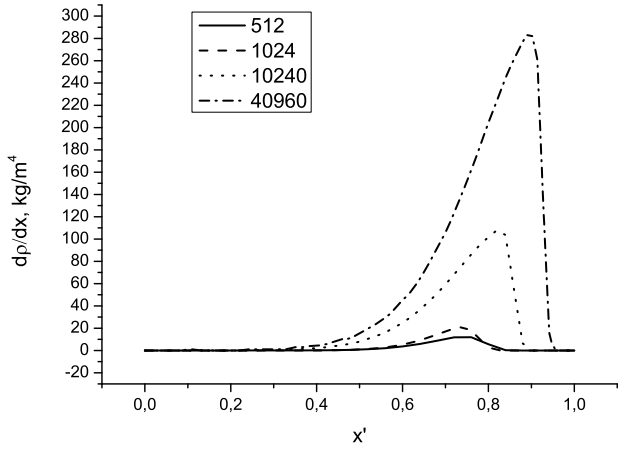

Figure 3. Spatial density gradient at $t = 2.0 \times 10^{-4}$ s. Numerals in explanatory legend correspond to various number of computational points.

right border we set free outflow condition. Figure 2 shows the gradient zone of the pressure wave, moving from the left boundary at $t = 2.0 \times 10^{-4}$ s for a different number of calculation points without any numerical oscillations either at the bottom of the wave or on the plateau behind it.

Density gradient as function of computational points number is shown in figure 3. Spatial range corresponding to the gradient zone is normalized to unity in order to show resolution of discontinuity, that is to say disruption "smearing" over finite number of cells.

3. The isothermal flow of a viscous weakly compressible fluid in a flat channel

With a view of successive complication let us consider the CABARET method implementation for the isothermal flow of Newtonian fluid in plane channel. The calculation was carried out basing OpenMP parallel computing library and developers' recommendations [2].

3.1. Algorithm formulation

Similarly to the previous section we start from governing equations written in divergence form:

$$\frac{\partial \rho}{\partial t} + \frac{\partial \rho u}{\partial x} + \frac{\partial \rho v}{\partial y} = 0, \tag{28}$$

$$\frac{\partial \rho u}{\partial t} + \frac{\partial \rho u^2}{\partial x} + \frac{\partial \rho uv}{\partial y} + \frac{\partial p}{\partial x} = \Lambda_u U, \tag{29}$$

$$\frac{\partial \rho v}{\partial t} + \frac{\partial \rho uv}{\partial x} + \frac{\partial \rho v^2}{\partial y} + \frac{\partial p}{\partial y} = \Lambda_v V. \tag{30}$$

One can write the viscous tensor $\overset{\leftrightarrow}{T} = \mu[\nabla v + (\nabla v)^T]$ utilising the notation

$$q_x^u = \frac{\partial u}{\partial x}, \quad q_y^u = \frac{\partial u}{\partial y}, \quad q_x^v = \frac{\partial v}{\partial x}, \quad q_y^v = \frac{\partial v}{\partial y}, \tag{31}$$

and neglecting the influence of compressibility in the following form:

$$\begin{aligned} \Lambda_u U &= \left(\frac{\partial \mu q_x^u}{\partial x} + \frac{\partial \mu q_y^u}{\partial y} \right), \\ \Lambda_v V &= \left(\frac{\partial \mu q_x^v}{\partial x} + \frac{\partial \mu q_y^v}{\partial y} \right). \end{aligned} \tag{32}$$

Then we rewrite the homogeneous equations in characteristic form. Unlike one-dimensional implemetation there are three different invariants, corresponding to two perpendicular directions. Column vector

$$\vec{\phi}^T = (\rho, u, v) \tag{33}$$

represents the set of independent variables for hyperbolic simultaneous equations

$$\frac{\partial \vec{\phi}}{\partial t} + A_x \frac{\partial \vec{\phi}}{\partial t} + A_y \frac{\partial \vec{\phi}}{\partial y} = 0, \tag{34}$$

where matrices $A_x = \begin{pmatrix} u & c^2\rho & 0 \\ \frac{1}{\rho} & u & 0 \\ 0 & 0 & u \end{pmatrix}$, $A_y = \begin{pmatrix} v & 0 & c^2\rho \\ 0 & v & 0 \\ \frac{1}{\rho} & 0 & v \end{pmatrix}$ possessing corresponding eigenvalues and eigenvectors:

$$\lambda_1^x = u + c, \quad \lambda_2^x = u - c, \quad \lambda_3^x = u, \tag{35}$$

$$\omega_1^x = \begin{pmatrix} 1/\rho c \\ 1 \\ 0 \end{pmatrix}, \quad \omega_2^x = \begin{pmatrix} -1/\rho c \\ 1 \\ 0 \end{pmatrix}, \quad \omega_3^x = \begin{pmatrix} 0 \\ 0 \\ 1 \end{pmatrix}, \tag{36}$$

$$\lambda_1^y = v + c, \quad \lambda_2^y = v - c, \quad \lambda_3^y = v, \tag{37}$$

$$\omega_1^y = \begin{pmatrix} 1/\rho c \\ 0 \\ 1 \end{pmatrix}, \quad \omega_2^y = \begin{pmatrix} -1/\rho c \\ 0 \\ 1 \end{pmatrix}, \quad \omega_3^y = \begin{pmatrix} 0 \\ 1 \\ 0 \end{pmatrix}. \tag{38}$$

Thus, homogeneous differential equations

$$\begin{aligned} \frac{\partial\vec{\phi}}{\partial t} + A_x\frac{\partial\vec{\phi}}{\partial x} = Q_x, \quad Q_x = -A_y\frac{\partial\vec{\phi}}{\partial y}, \\ \frac{\partial\vec{\phi}}{\partial t} + A_y\frac{\partial\vec{\phi}}{\partial y} = Q_y, \quad Q_y = -A_x\frac{\partial\vec{\phi}}{\partial x} \end{aligned} \tag{39}$$

have characteristic form

$$\frac{\partial I_k^x}{\partial t} + \lambda_k^x\frac{\partial I_k^x}{\partial x} = G_k^x, \quad \frac{\partial I_k^y}{\partial t} + \lambda_x^k\frac{\partial I_k^y}{\partial x} = G_k^y, \quad k = 1,2,3, \tag{40}$$

where the number of familiar Riemann invariants I_k^i increases:

$$I_1^x = c\ln(p + c^2\rho_0) + u, \quad I_2^x = -c\ln(p + c^2\rho_0) + u, \quad I_3^x = v, \tag{41}$$

$$I_1^y = c\ln(p + c^2\rho_0) + v, \quad I_2^y = -c\ln(p + c^2\rho_0) + v, \quad I_3^y = u. \tag{42}$$

For a two-dimensional implementation the main algorithm is to be modified.

(i) Firstly, n-th layer conservative and flux variables are initialized in accordance with initial values so that the divergence of velocity is zero.

(ii) Secondly, an optimal sound speed should be determined basing the following reasoning. If the flow time is less $t_1 = 3\max(L_X, L_Y)/C_{\text{init}}$, where L_X and L_Y stand for X and Y direction domain size, sound speed $C_{\text{init}} = 10.0$–1500.0 m/s given in a setup file remains unchanged over this time span in order to complete the process of pressure wave propagation (compression towards the outlet, as well as backward rarefaction wave and accompanying them velocity waves). When the timer expires t_1 the sound speed c is determined as $c^{n+1} = 10\max(|U^n|, |V^n|, |u^n|, |v^n|)$. The new value is accepted, if $c_{\text{visc}} < c^{n+1} < C_{\text{init}}$, wherein $c_{\text{visc}} = 2\min(\Delta x, \Delta y)\rho_0/\mu_0$ denotes momentum transfer speed (hydrodynamic mode). In case of $c \le c_{\text{visc}}$ sound speed is set $c = 10c_{\text{visc}}$. However, c can not be greater than that of in real fluid ($c \approx 1500.0$ m/s).

(iii) Thirdly, the time step is calculated relying on the extended numerical stability condition $\tau = \text{CFL}h\min(1/c, 2h\rho/\mu)$, where $h = \min(\Delta x, \Delta y)$.

(iv) Next, we calculate conservative variables at the intermediate layer in accordance with

$$\frac{{}^{n+\frac12}[\mathbb{R}]_{j+\frac12}^{i+\frac12} - {}^{n}[\mathbb{R}]_{j+\frac12}^{i+\frac12}}{\tau_{n+\frac12}/2} + \frac{{}^{n}[\rho u]_{j+\frac12}^{i+1} - {}^{n}[\rho u]_{j+\frac12}^{i}}{\Delta x_{i+\frac12}} + \frac{{}^{n}[\rho v]_{j+1}^{i+\frac12} - {}^{n}[\rho v]_{j}^{i+\frac12}}{\Delta y_{j+\frac12}} = 0, \tag{43}$$

$$\frac{{}^{n+\frac12}[\mathbb{R}U]_{j+\frac12}^{i+\frac12} - {}^{n}[\mathbb{R}U]_{j+\frac12}^{i+\frac12}}{\tau_{n+\frac12}/2} + \frac{{}^{n}[\rho u^2 + p]_{j+\frac12}^{i+1} - {}^{n}[\rho u^2 + p]_{j+\frac12}^{i}}{\Delta x_{i+\frac12}} + \frac{{}^{n}[\rho uv]_{j+1}^{i+\frac12} - {}^{n}[\rho uv]_{j}^{i+\frac12}}{\Delta y_{j+\frac12}} = 0, \tag{44}$$

$$\frac{{}^{n+\frac12}[\mathbb{R}V]_{j+\frac12}^{i+\frac12} - {}^{n}[\mathbb{R}V]_{j+\frac12}^{i+\frac12}}{\tau_{n+\frac12}/2} + \frac{{}^{n}[\rho uv]_{j+\frac12}^{i+1} - {}^{n}[\rho uv]_{j+\frac12}^{i}}{\Delta x_{i+\frac12}} + \frac{{}^{n}[\rho v^2 + p]_{j+1}^{i+\frac12} - {}^{n}[\rho v^2 + p]_{j}^{i+\frac12}}{\Delta y_{j+\frac12}} = 0. \tag{45}$$

The indices i and j in (43)–(45) and further numerate points in X and Y directions correspondingly, n denotes time layer number, the indices $i+1/2$, and $j+1/2$ are referred to flux-type variables and located at midpoints of cells facets, $n+1/2$ relates only to the conservative variables of the intermediate time layer.

(v) Then one need to calculate conservative variables at the same time layer with respect to inhomogeneous FDE

$$
\begin{aligned}
{}^{n+\frac{1}{2}}[\mathbb{P}]^{i+\frac{1}{2}}_{j+\frac{1}{2}} \frac{{}^{n+\frac{1}{2}}[\tilde{U}]^{i+\frac{1}{2}}_{j+\frac{1}{2}} - {}^{n+\frac{1}{2}}[U]^{i+\frac{1}{2}}_{j+\frac{1}{2}}}{\tau_{n+\frac{1}{2}}/2} &= \Lambda^h U^n, \\
{}^{n+\frac{1}{2}}[\mathbb{P}]^{i+\frac{1}{2}}_{j+\frac{1}{2}} \frac{{}^{n+\frac{1}{2}}[\tilde{V}]^{i+\frac{1}{2}}_{j+\frac{1}{2}} - {}^{n+\frac{1}{2}}[V]^{i+\frac{1}{2}}_{j+\frac{1}{2}}}{\tau_{n+\frac{1}{2}}/2} &= \Lambda^h V^n,
\end{aligned}
\tag{46}
$$

wherein the following notation is introduced:

$$
\Lambda^h U^n = \frac{1}{\Delta x_{i+\frac{1}{2}}} \left({}^{n}[\mu]^{i+\frac{1}{2}}_{j+\frac{1}{2}} \left({}^{n}[q^u_x]^{i+1}_{j+\frac{1}{2}} - {}^{n}[q^u_x]^{i}_{j+\frac{1}{2}} \right) \right) + \frac{1}{\Delta y_{j+\frac{1}{2}}} \left({}^{n}[\mu]^{i+\frac{1}{2}}_{j+\frac{1}{2}} \left({}^{n}[q^u_y]^{i+\frac{1}{2}}_{j+1} - {}^{n}[q^u_y]^{i+\frac{1}{2}}_{j} \right) \right), \tag{47}
$$

$$
\Lambda^h V^n = \frac{1}{\Delta x_{i+\frac{1}{2}}} \left({}^{n}[\mu]^{i+\frac{1}{2}}_{j+\frac{1}{2}} \left({}^{n}[q^v_x]^{i+1}_{j+\frac{1}{2}} - {}^{n}[q^v_x]^{i}_{j+\frac{1}{2}} \right) \right) + \frac{1}{\Delta y_{j+\frac{1}{2}}} \left({}^{n}[\mu]^{i+\frac{1}{2}}_{j+\frac{1}{2}} \left({}^{n}[q^v_y]^{i+\frac{1}{2}}_{j+1} - {}^{n}[q^u_y]^{i+\frac{1}{2}}_{j} \right) \right), \tag{48}
$$

and the fluxes belonging to the internal cells centers ($i = 1 \dots n_X - 1, j = 1 \dots n_Y - 1$) determined from the formulae:

$$
\begin{aligned}
{}^{n}[q^u_x]^{i}_{j+\frac{1}{2}} &= \frac{{}^{n}[U]^{i+\frac{1}{2}}_{j+\frac{1}{2}} - {}^{n}[U]^{i-\frac{1}{2}}_{j+\frac{1}{2}}}{\Delta x_i}, \quad & {}^{n}[q^u_y]^{i+\frac{1}{2}}_{j} &= \frac{{}^{n}[U]^{i+\frac{1}{2}}_{j+\frac{1}{2}} - {}^{n}[U]^{i+\frac{1}{2}}_{j-\frac{1}{2}}}{\Delta y_i}, \\
{}^{n}[q^v_x]^{i}_{j+\frac{1}{2}} &= \frac{{}^{n}[V]^{i+\frac{1}{2}}_{j+\frac{1}{2}} - {}^{n}[V]^{i-\frac{1}{2}}_{j+\frac{1}{2}}}{\Delta x_i}, \quad & {}^{n}[q^v_y]^{i+\frac{1}{2}}_{j} &= \frac{{}^{n}[V]^{i+\frac{1}{2}}_{j+\frac{1}{2}} - {}^{n}[V]^{i+\frac{1}{2}}_{j-\frac{1}{2}}}{\Delta y_i}.
\end{aligned}
\tag{49}
$$

To calculate the fluxes in boundary cells one can use the value of the adjacent flux-type variables, that leads to additional factor 2 in

$$
\begin{aligned}
{}^{n}[q^u_x]^{1}_{j+\frac{1}{2}} &= 2\frac{{}^{n}[U]^{\frac{1}{2}}_{j+\frac{1}{2}} - {}^{n}[u]^{0}_{j+\frac{1}{2}}}{\Delta x_i}, \quad & {}^{n}[q^u_x]^{\mathrm{n_X}}_{j+\frac{1}{2}} &= 2\frac{{}^{n}[u]^{\mathrm{n_X}}_{j+\frac{1}{2}} - {}^{n}[u]^{n_X-\frac{1}{2}}_{j+\frac{1}{2}}}{\Delta x_i}, \\
{}^{n}[q^u_y]^{i+\frac{1}{2}}_{1} &= 2\frac{{}^{n}[U]^{i+\frac{1}{2}}_{\frac{1}{2}} - {}^{n}[u]^{i+\frac{1}{2}}_{0}}{\Delta y_i}, \quad & {}^{n}[q^u_y]^{i+\frac{1}{2}}_{\mathrm{n_Y}} &= 2\frac{{}^{n}[u]^{i+\frac{1}{2}}_{\mathrm{n_Y}} - {}^{n}[U]^{i+\frac{1}{2}}_{n_Y-\frac{1}{2}}}{\Delta y_i}, \\
{}^{n}[q^v_x]^{1}_{j+\frac{1}{2}} &= 2\frac{{}^{n}[V]^{\frac{1}{2}}_{j+\frac{1}{2}} - {}^{n}[v]^{0}_{j+\frac{1}{2}}}{\Delta x_i}, \quad & {}^{n}[q^v_x]^{\mathrm{n_X}}_{j+\frac{1}{2}} &= 2\frac{{}^{n}[v]^{\mathrm{n_X}}_{j+\frac{1}{2}} - {}^{n}[V]^{n_X-\frac{1}{2}}_{j+\frac{1}{2}}}{\Delta x_i}, \\
{}^{n}[q^v_y]^{i+\frac{1}{2}}_{1} &= 2\frac{{}^{n}[V]^{i+\frac{1}{2}}_{\frac{1}{2}} - {}^{n}[v]^{i+\frac{1}{2}}_{0}}{\Delta y_i}, \quad & {}^{n}[q^v_y]^{i+\frac{1}{2}}_{\mathrm{n_Y}} &= 2\frac{{}^{n}[v]^{i+\frac{1}{2}}_{\mathrm{n_Y}} - {}^{n}[V]^{i+\frac{1}{2}}_{n_Y-\frac{1}{2}}}{\Delta y_i}.
\end{aligned}
\tag{50}
$$

(vi) On the next step we are to find the new values for flux-type variables in internal cells. As weakly compressible fluid flow is always subsonic, the values of the first kind invariant are transferred from left to right, and vice versa for the second invariant. So one should extrapolate I_1^x to the new layer by formula

$$ {}^{n+1}[I_1^x]^i_{j+\frac{1}{2}} = 2^{n+\frac{1}{2}}[I_1^x]^{i-\frac{1}{2}}_{j+\frac{1}{2}} -^n [I_1^x]^{i-1}_{j+\frac{1}{2}}, \tag{51} $$

using left-hand side (LHS) conservative variables on the intermediate layer

$$ {}^{n+\frac{1}{2}}[I_1^x]^{i-\frac{1}{2}}_{j+\frac{1}{2}} = c^n \ln\left(p({}^{n+\frac{1}{2}}[\mathbb{R}]^{i-\frac{1}{2}}_{j+\frac{1}{2}}) + c^2\rho_0\right) +^{n+\frac{1}{2}} [\mathbb{U}]^{i-\frac{1}{2}}_{j+\frac{1}{2}}, \tag{52} $$

LHS flux-type ones at the preceding time layer

$$ {}^{n}[I_1^x]^{i-1}_{j+\frac{1}{2}} = c^n \ln\left(p({}^{n}[\mathbb{R}]^{i-1}_{j+\frac{1}{2}}) + c^2\rho_0\right) +^{n} [\mathbb{U}]^{i-1}_{j+\frac{1}{2}}. \tag{53} $$

Again, to implement nonlinear correction algorithm we also are to calculate invariants based on LHS conservative variables at the preceeding layer:

$$ {}^{n}[I_1^x]^{i-\frac{1}{2}}_{j+\frac{1}{2}} = c^n \ln\left(p({}^{n}[\mathbb{R}]^{i-\frac{1}{2}}_{j+\frac{1}{2}}) + c^2\rho_0\right) +^{n} [\mathbb{U}]^{i-\frac{1}{2}}_{j+\frac{1}{2}}, \tag{54} $$

and flux-type variables at the current point:

$$ {}^{n-1}[I_1^x]^{i}_{j+\frac{1}{2}} = c^n \ln\left(p({}^{n-1}[\mathbb{R}]^{i}_{j+\frac{1}{2}}) + c^2\rho_0\right) +^{n-1} [\mathbb{U}]^{i}_{j+\frac{1}{2}}. \tag{55} $$

Proceeding from known invariants set we also extrapolate right-hand side (RHS) parts of inhomogeneous transfer equations in characteristic form:

$$ {}^{n+\frac{1}{2}}\langle G_1^x\rangle^{i-\frac{1}{2}}_{j+\frac{1}{2}} = \frac{{}^{n+\frac{1}{2}}[I_1^x]^{i-\frac{1}{2}}_{j+\frac{1}{2}} -^n [I_1^x]^{i-\frac{1}{2}}_{j+\frac{1}{2}}}{\tau_{n+\frac{1}{2}}/2} +^{n+\frac{1}{2}} [\lambda]^{i-\frac{1}{2}}_{j+\frac{1}{2}} \frac{{}^{n}[I_1^x]^{i}_{j+\frac{1}{2}} -^n [I_1^x]^{i-1}_{j+\frac{1}{2}}}{\Delta x_{i+\frac{1}{2}}}. \tag{56} $$

Guided by general procedure we are to perform a nonlinear correction of the first kind invariant as follows:

$$ {}^{n+1}[I_1^x]^i_{j+\frac{1}{2}} = \begin{cases} {}^{n+1}[I_1^x]^i_{j+\frac{1}{2}}, & \text{if } \min(I_1^x) \le^{n+1} [I_1^x]^i_{j+\frac{1}{2}} \le \max(I_1^x) \\ \min(I_1^x), & \text{if } {}^{n+1}[I_1^x]^i_{j+\frac{1}{2}} < \min(I_1^x) \\ \max(I_1^x), & \text{if } {}^{n+1}[I_1^x]^i_{j+\frac{1}{2}} > \max(I_1^x) \end{cases}, \quad l = 1, 2, \tag{57} $$

wherein

$$ \begin{aligned} \max(I_1^x) &= \max\left\{{}^{n}[I_1^x]^{i-1}_{j+\frac{1}{2}}, \quad {}^{n}[I_1^x]^{i-\frac{1}{2}}_{j+\frac{1}{2}}, \quad {}^{n}[I_1^x]^{i}_{j+\frac{1}{2}}\right\} + \tau^{n+\frac{1}{2}}_{n+\frac{1}{2}}\langle G_1^x\rangle^{i-\frac{1}{2}}_{j+\frac{1}{2}}, \\ \min(I_1^x) &= \min\left\{{}^{n}[I_1^x]^{i-1}_{j+\frac{1}{2}}, \quad {}^{n}[I_1^x]^{i-\frac{1}{2}}_{j+\frac{1}{2}}, \quad {}^{n}[I_1^x]^{i}_{j+\frac{1}{2}}\right\} + \tau^{n+\frac{1}{2}}_{n+\frac{1}{2}}\langle G_1^x\rangle^{i-\frac{1}{2}}_{j+\frac{1}{2}}. \end{aligned} \tag{58} $$

In a similar way one can calculate the second kind invariant using RHS cell parameters such as RHS (in the center of adjacent cell) conservative variables at the intermediate time layer

$$ {}^{n+\frac{1}{2}}[I_2^x]^{i+1\frac{1}{2}}_{j+\frac{1}{2}} = c^n \ln\left(p({}^{n+\frac{1}{2}}[\mathbb{R}]^{i+\frac{1}{2}}_{j+\frac{1}{2}}) + c^2\rho_0\right) +^{n+\frac{1}{2}} [\mathbb{U}]^{i+\frac{1}{2}}_{j+\frac{1}{2}} \tag{59} $$

and RHS flux-type variables at the preceding time layer

$$ {}^{n}[I_2^x]_{j+\frac{1}{2}}^{i+1} = c^n \ln\left(p({}^{n}[\mathbb{R}]_{j+\frac{1}{2}}^{i+1}) + c^2\rho_0\right) +^{n} [\mathbb{U}]_{j+\frac{1}{2}}^{i+1} \tag{60} $$

in the underlying approximation

$$ {}^{n+1}[I_2^x]_{j+\frac{1}{2}}^{i} = 2^{n+\frac{1}{2}}[I_2^x]_{j+\frac{1}{2}}^{i+\frac{1}{2}} -^{n} [I_2^x]_{j+\frac{1}{2}}^{i+1}. \tag{61} $$

So far, to obtain reasonable invariant value we perform routine nonlinear correction

$$ {}^{n+1}[I_2^x]_{j+\frac{1}{2}}^{i} = \begin{cases} {}^{n+1}[I_2^x]_{j+\frac{1}{2}}^{i}, & \text{if } \min(I_2^x) \le^{n+1} [I_2^x]_{j+\frac{1}{2}}^{i} \le \max(I_2^x) \\ \min(I_2^x), & \text{if } {}^{n+1}[I_2^x]_{j+\frac{1}{2}}^{i} < \min(I_2^x) \\ \max(I_2^x), & \text{if } {}^{n+1}[I_2^x]_{j+\frac{1}{2}}^{i} > \max(I_2^x) \end{cases}, \tag{62} $$

wherein ${}^{n}[I_2^x]_{j+\frac{1}{2}}^{i+\frac{1}{2}}$ is rested upon preceding layer RHS conservative variables

$$ {}^{n}[I_2^x]_{j+\frac{1}{2}}^{i+\frac{1}{2}} = c^n \ln\left(p({}^{n}[\mathbb{R}]_{j+\frac{1}{2}}^{i+\frac{1}{2}})\right) +^{n} [\mathbb{U}]_{j+\frac{1}{2}}^{i+\frac{1}{2}}, \tag{63} $$

${}^{n-1}[I_2^x]_{j+\frac{1}{2}}^{i}$ is determined by former layer RHS flux-type variables:

$$ {}^{n}[I_2^x]_{j+\frac{1}{2}}^{i} = c^n \ln\left(p({}^{n-1}[\mathbb{R}]_{j+\frac{1}{2}}^{i})\right) +^{n} [\mathbb{U}]_{j+\frac{1}{2}}^{i} \tag{64} $$

and

$$ {}^{n+\frac{1}{2}}\langle G_2^x\rangle_{j+\frac{1}{2}}^{i+\frac{1}{2}} = \frac{{}^{n+\frac{1}{2}}[I_2^x]_{j+\frac{1}{2}}^{i+\frac{1}{2}} -^{n} [I_2^x]_{j+\frac{1}{2}}^{i+\frac{1}{2}}}{\tau_{n+\frac{1}{2}}/2} +^{n+\frac{1}{2}} [\lambda]_{j+\frac{1}{2}}^{i+\frac{1}{2}} \frac{{}^{n}[I_2^x]_{j+\frac{1}{2}}^{i} -^{n} [I_2^x]_{j+\frac{1}{2}}^{i+1}}{\Delta x_{i+\frac{1}{2}}} \tag{65} $$

$$ \begin{aligned} \max(I_2^x) &= \max\left\{{}^{n}[I_2^x]_{j+\frac{1}{2}}^{i+1}, \quad {}^{n}[I_2^x]_{j+\frac{1}{2}}^{i+\frac{1}{2}}, \quad {}^{n}[I_2^x]_{j+\frac{1}{2}}^{i}\right\} + \tau_{n+\frac{1}{2}}^{n+\frac{1}{2}}\langle G_2^x\rangle_{j+\frac{1}{2}}^{i+\frac{1}{2}}, \\ \min(I_2^x) &= \min\left\{{}^{n}[I_2^x]_{j+\frac{1}{2}}^{i+1}, \quad {}^{n}[I_2^x]_{j+\frac{1}{2}}^{i+\frac{1}{2}}, \quad {}^{n}[I_2^x]_{j+\frac{1}{2}}^{i}\right\} + \tau_{n+\frac{1}{2}}^{n+\frac{1}{2}}\langle G_2^x\rangle_{j+\frac{1}{2}}^{i+\frac{1}{2}}. \end{aligned} \tag{66} $$

Invariants at the new layer now let us find flux-type variables ${}^{n+1}[p]_{j+\frac{1}{2}}^{i}$,${}^{n+1}[u]_{j+\frac{1}{2}}^{i}$, the former one is used as a switch, since it determines which of two adjacent cells (left or right) will be employed to extrapolate and correct the third invariant. A positive value of flux-type velocity ${}^{n+1}[u]_{j+\frac{1}{2}}^{i} \ge 0$, means that we will exploit LHS cell parameters:

$$ {}^{n+1}[I_3^x]_{j+\frac{1}{2}}^{i} = 2^{n+\frac{1}{2}}[I_3^x]_{j+\frac{1}{2}}^{i-\frac{1}{2}} -^{n} [I_3^x]_{j+\frac{1}{2}}^{i-1}, \tag{67} $$

$$ {}^{n+1}[I_3^x]_{j+\frac{1}{2}}^{i} = \begin{cases} {}^{n+1}[I_3^x]_{j+\frac{1}{2}}^{i}, & \text{if } \min(I_3^x) \le^{n+1} [I_3^x]_{j+\frac{1}{2}}^{i} \le \max(I_3^x) \\ \min(I_3^x), & \text{if } {}^{n+1}[I_3^x]_{j+\frac{1}{2}}^{i} < \min(I_3^x) \\ \max(I_3^x), & \text{if } {}^{n+1}[I_3^x]_{j+\frac{1}{2}}^{i} > \max(I_3^x) \end{cases}, \tag{68} $$

wherein

$$\begin{aligned}
\max(I_3^x) &= \max\left\{{}^n[I_3^x]^{i-1}_{j+\frac{1}{2}}, \quad {}^n[I_3^x]^{i-\frac{1}{2}}_{j+\frac{1}{2}}, \quad {}^n[I_3^x]^{i}_{j+\frac{1}{2}}\right\} + \tau^{n+\frac{1}{2}}_{n+\frac{1}{2}}\langle G_3^x\rangle^{i-\frac{1}{2}}_{j+\frac{1}{2}},\\
\min(I_3^x) &= \min\left\{{}^n[I_3^x]^{i-1}_{j+\frac{1}{2}}, \quad {}^n[I_3^x]^{i-\frac{1}{2}}_{j+\frac{1}{2}}, \quad {}^n[I_3^x]^{i}_{j+\frac{1}{2}}\right\} + \tau^{n+\frac{1}{2}}_{n+\frac{1}{2}}\langle G_3^x\rangle^{i-\frac{1}{2}}_{j+\frac{1}{2}},\\
{}^{n+\frac{1}{2}}\langle G_3^x\rangle^{i-\frac{1}{2}}_{j+\frac{1}{2}} &= \frac{{}^{n+\frac{1}{2}}[I_3^x]^{i-\frac{1}{2}}_{j+\frac{1}{2}} - {}^n[I_3^x]^{i-\frac{1}{2}}_{j+\frac{1}{2}}}{\tau_{n+\frac{1}{2}}/2} + {}^{n+\frac{1}{2}}[\lambda_3^x]^{i-\frac{1}{2}}_{j+\frac{1}{2}}\frac{{}^n[I_3^x]^{i}_{j+\frac{1}{2}} - {}^n[I_3^x]^{i-1}_{j+\frac{1}{2}}}{\Delta x_{i+\frac{1}{2}}}.
\end{aligned} \tag{69}$$

Coversely, ${}^{n+1}_{i}[u]^{k+\frac{1}{2}}_{j+\frac{1}{2}} < 0$ leads us to RHS cell:

$${}^{n+1}[I_3^x]^{i}_{j+\frac{1}{2}} = 2^{n+\frac{1}{2}}[I_3^x]^{i+\frac{1}{2}}_{j+\frac{1}{2}} - {}^n[I_3^x]^{i+1}_{j+\frac{1}{2}}, \tag{70}$$

$${}^{n+1}[I_3^x]^{i}_{j+\frac{1}{2}} = \begin{cases} {}^{n+1}[I_3^x]^{i}_{j+\frac{1}{2}}, & \text{if } \min(I_3^x) \le {}^{n+1}[I_3^x]^{i}_{j+\frac{1}{2}} \le \max(I_3^x)\\ \min(I_3^x), & \text{if } {}^{n+1}[I_3^x]^{i}_{j+\frac{1}{2}} < \min(I_3^x)\\ \max(I_3^x), & \text{if } {}^{n+1}[I_3^x]^{i}_{j+\frac{1}{2}} > \max(I_3^x) \end{cases}, \tag{71}$$

wherein

$$\begin{aligned}
\max(I_3^x) &= \max\left\{{}^n[I_3^x]^{i+1}_{j+\frac{1}{2}}, \quad {}^n[I_3^x]^{i+\frac{1}{2}}_{j+\frac{1}{2}}, \quad {}^n[I_3^x]^{i}_{j+\frac{1}{2}}\right\} + \tau^{n+\frac{1}{2}}_{n+\frac{1}{2}}\langle G_3^x\rangle^{i+\frac{1}{2}}_{j+\frac{1}{2}},\\
\min(I_3^x) &= \min\left\{{}^n[I_3^x]^{i+1}_{j+\frac{1}{2}}, \quad {}^n[I_3^x]^{i+\frac{1}{2}}_{j+\frac{1}{2}}, \quad {}^n[I_3^x]^{i}_{j+\frac{1}{2}}\right\} + \tau^{n+\frac{1}{2}}_{n+\frac{1}{2}}\langle G_3^x\rangle^{i+\frac{1}{2}}_{j+\frac{1}{2}},\\
{}^{n+\frac{1}{2}}\langle G_3^x\rangle^{i+\frac{1}{2}}_{j+\frac{1}{2}} &= \frac{{}^{n+\frac{1}{2}}[I_3^x]^{i+\frac{1}{2}}_{j+\frac{1}{2}} - {}^n[I_3^x]^{i+\frac{1}{2}}_{j+\frac{1}{2}}}{\tau_{n+\frac{1}{2}}/2} + {}^{n+\frac{1}{2}}[\lambda]^{i+\frac{1}{2}}_{j+\frac{1}{2}}\frac{{}^n[I_3^x]^{i+1}_{j+\frac{1}{2}} - {}^n[I_3^x]^{i}_{j+\frac{1}{2}}}{\Delta x_{i+\frac{1}{2}}}.
\end{aligned} \tag{72}$$

Then from above equations we determine the deficient values of flux-type variables. Calculation procedure for flux-type variables responsible for transport in Y direction is fully identical.

(vii) Boundary cells flux-type variables are considered in terms of corresponding boundary values. One can set 5 various types of boundary conditions for every edge, such as impermeability (*1*), no-slip (*2*), subsonic inlet (*3*), free outflow (*4*), periodic (*5*) conditions.
In present paper we use plane Poiseuille flow as a test problem. It is worth noting that in CABARET method we are to set boundary conditions for Riemann invariants, i.e. to specify far-field parameters ${}^{n+1}p_\infty$, ${}^{n+1}u_\infty$, ${}^{n+1}v_\infty$ determining first kind invariant. So for the internal cell parameters we find the second kind invariant value coming to the front boundary from the interior. To approximate RHS terms of transfer equations one should use an averaged value of characteristic number:

$${}^{n+\frac{1}{2}}[\lambda_2^x]^0_{j+\frac{1}{2}} = \frac{1}{2}\left({}^{n+1}u_\infty + {}^{n+\frac{1}{2}}[U]^{\frac{1}{2}}_{j+\frac{1}{2}}\right) + c.$$

The third variant calculation approach depends on the sign of averaged characteristic velocity

$${}^{n+\frac{1}{2}}[\lambda_3^x]^0_{j+\frac{1}{2}} = \frac{1}{2}\left({}^{n+\frac{1}{2}}U^{\frac{1}{2}}_{j+\frac{1}{2}} + {}^{n+1}u_\infty\right), \tag{73}$$

and if ${}^{n+\frac{1}{2}}[\lambda_3^x]_{j+\frac{1}{2}}^0 \geq 0$, then ${}^{n+1}[v]_{j+\frac{1}{2}}^0 = {}^{n+1}\left[I_3^x\right]_{j+\frac{1}{2}}^0$. Otherwise, ${}^{n+1}[v]_{j+\frac{1}{2}}^0$ is obtained from LHS cell parameters.

The free outlet condition at the back wall requires both quasi-steady Mach number and the characteristic number that for the case of weakly compressible fluid results into

$$ {}^{n+1}[u]_{j+\frac{1}{2}}^{\mathrm{n_X}} = {}^{n+1}[U]_{j+\frac{1}{2}}^{n_X-\frac{1}{2}}. $$

To find back wall boundary value for density we need to calculate ${}^{n+1}[I_1^x]_{j+\frac{1}{2}}^{\mathrm{n_X}}$. As for the third invariant, we assign its value in accordance with the sign of ${}^{n+\frac{1}{2}}[\lambda_3^x]_{j+\frac{1}{2}}^{n_X+\frac{1}{2}}$. At the left boundary we set no-slip condition wherein all flux-type velocity components are equal to zero: ${}^{n+1}[u]_0^{i+\frac{1}{2}} = {}^{n+1}[v]_0^{i+\frac{1}{2}} = 0$, a further condition comes with the second kind characteristics

$$ -c\ln\left({}^{n+1}[p]_0^{i+\frac{1}{2}} + c^2\rho_0\right) = {}^{n+1}[I_2^y]_0^{i+\frac{1}{2}}. \tag{74} $$

The following formulae are also introduced for the right boundary:

$$ {}^{n+1}[u]_{\mathrm{n_Y}}^{i+\frac{1}{2}} = {}^{n+1}[v]_{\mathrm{n_Y}}^{i+\frac{1}{2}} = 0, \quad c\ln\left({}^{n+1}[p]_{\mathrm{n_Y}}^{i+\frac{1}{2}} + c^2\rho_0\right) = {}^{n+1}[I_1^y]_0^{i+\frac{1}{2}}. \tag{75} $$

(viii) Moving to the final steps of the CABARET method, we now calculate conservative variables at the $(n+1)$-layer utilizing homogeneous FDE

$$ \frac{{}^{n+1}[\mathbb{R}]_{j+\frac{1}{2}}^{i+\frac{1}{2}} - {}^{n}\left[\mathbb{R}\right]_{j+\frac{1}{2}}^{i+\frac{1}{2}}}{\tau_{n+\frac{1}{2}}} + \frac{{}^{n}[\overline{\rho u}]_{j+\frac{1}{2}}^{i+1} - {}^{n}\left[\overline{\rho u}\right]_{j+\frac{1}{2}}^{i}}{\Delta x_{i+\frac{1}{2}}} + \frac{{}^{n}[\overline{\rho v}]_{j+1}^{i+\frac{1}{2}} - {}^{n}\left[\overline{\rho v}\right]_{j}^{i+\frac{1}{2}}}{\Delta y_{j+\frac{1}{2}}} = 0, \tag{76} $$

$$ \frac{{}^{n+1}[\mathbb{R}U]_{j+\frac{1}{2}}^{i+\frac{1}{2}} - {}^{n}\left[\mathbb{R}U\right]_{j+\frac{1}{2}}^{i+\frac{1}{2}}}{\tau_{n+\frac{1}{2}}} + \frac{{}^{n}[\overline{\rho u^2+p}]_{j+\frac{1}{2}}^{i+1} - {}^{n}\left[\overline{\rho u^2+p}\right]_{j+\frac{1}{2}}^{i}}{\Delta x_{n+\frac{1}{2}}} + \frac{{}^{n}[\overline{\rho uv}]_{j+1}^{i+\frac{1}{2}} - {}^{n}\left[\overline{\rho uv}\right]_{j}^{i+\frac{1}{2}}}{\Delta y_{n+\frac{1}{2}}} = 0, \tag{77} $$

$$ \frac{{}^{n+1}[\mathbb{R}V]_{j+\frac{1}{2}}^{i+\frac{1}{2}} - {}^{n}\left[\mathbb{R}V\right]_{j+\frac{1}{2}}^{i+\frac{1}{2}}}{\tau_{n+\frac{1}{2}}} + \frac{{}^{n}[\overline{\rho uv}]_{j+\frac{1}{2}}^{i+1} - {}^{n}\left[\overline{\rho uv}\right]_{j+\frac{1}{2}}^{i}}{\Delta x_{i+\frac{1}{2}}} + \frac{{}^{n}[\overline{\rho v^2+p}]_{j+1}^{i+\frac{1}{2}} - {}^{n}\left[\overline{\rho v^2+p}\right]_{j}^{i+\frac{1}{2}}}{\Delta y_{j+\frac{1}{2}}} = 0. \tag{78} $$

(ix) To finish current time step we correct new conservative variables with respect to viscous forces:

$$ \begin{aligned} {}^{n+1}[\mathbb{R}]_{j+\frac{1}{2}}^{i+\frac{1}{2}} \frac{{}^{n+\frac{1}{2}}[\tilde{U}]_{j+\frac{1}{2}}^{i+\frac{1}{2}} - {}^{n+\frac{1}{2}}\left[U\right]_{j+\frac{1}{2}}^{i+\frac{1}{2}}}{\tau_{n+\frac{1}{2}}} &= \Lambda^h U^{n+\frac{1}{2}}, \\ {}^{n+1}[\mathbb{R}]_{j+\frac{1}{2}}^{i+\frac{1}{2}} \frac{{}^{n+\frac{1}{2}}[\tilde{V}]_{j+\frac{1}{2}}^{i+\frac{1}{2}} - {}^{n+\frac{1}{2}}\left[V\right]_{j+\frac{1}{2}}^{i+\frac{1}{2}}}{\tau_{n+\frac{1}{2}}} &= \Lambda^h V^{n+\frac{1}{2}}. \end{aligned} \tag{79} $$

Viscous fluxes in the interior cells are determined by intermediate layer conservative variables, whereas for boundary cells we also employ time-averaged flux-type variables:

$$\overline{[u]}^{l}_{j+\frac{1}{2}} = 0.5\left({}^{n}[u]^{l}_{j+\frac{1}{2}} + {}^{n+1}[u]^{l}_{j+\frac{1}{2}}\right), \quad \overline{[v]}^{l}_{j+\frac{1}{2}} = 0.5\left({}^{n}[v]^{l}_{j+\frac{1}{2}} + {}^{n+1}[v]^{l}_{j+\frac{1}{2}}\right), \quad l = 1, n_X,$$

$$\overline{[u]}^{i+\frac{1}{2}}_{m} = 0.5\left({}^{n}[u]^{i+\frac{1}{2}}_{m} + {}^{n+1}[u]^{i+\frac{1}{2}}_{m}\right), \quad \overline{[v]}^{i+\frac{1}{2}}_{m} = 0.5\left({}^{n}[v]^{i+\frac{1}{2}}_{m} + {}^{n+1}[v]^{j+\frac{1}{2}}_{m}\right), \quad m = 1, n_Y.$$

3.2. Classical Poiseuille flow in a plane channel

A classical plane Poiseuille flow under the constant pressure gradient was used as a benchmark for the two-dimensional CABARET method. It's important to note again that according to general procedure we are to set the Riemann invariants according to boundary conditions. Thus, the far-field pressure coincides implicitly with a stagnation pressure in isentropic compressible fluid flows.

To set Poiseuille flow in the most accurate way we keep constant gradient condition deliberately specifying values of flux-type pressure variables at the boundaries. For calculation we use quite coarse grid with the number of cells $n_X = 60$, $n_Y = 100$. The following data are also necessary for equation solving: a sound velocity $c = 1.0$–100.0 m/s, a fluid viscosity $\mu = 0.1$ Pa s, a channel length $L_X = 2.0$ m, a channel width $L_Y = 0.1$ m, reference density $\rho_0 = 1000.0$ kg/m^3, both initial velocity components and pressure are set to be zero. Initial density of the equation of state, the components of the initial velocity and pressure are set equal to zero. We compared the results with the steady-state velocity profile determined by the formula

$$U(y) = \frac{\Delta p}{2\mu L_X} y(y - L_Y), \quad y \in [0, L_Y], \tag{80}$$

calculating the relative error ϵ between numerical U_c and analytical U_a values of streamwise axial velocity:

$$\epsilon = \frac{|U_c - U_a|}{U_a}. \tag{81}$$

The maximum this error shown in figure 4 for different values of static pressure differential Δp does not exceed 1.5% and appertains to an axial region for all calculations except for the first one. This fact stems from very slow stabilisation, that may be unfinished at flow time $t \approx 70$ s. However, in the first test performed for a very slow flow at $\Delta p = 1.6$ Pa and axial velocity $U_{\text{axial}} = 0.01$ m/s, the range of maximum error falls on boundary layers and does not exceed 0.5%. Generally speaking the errors obtained do not exceed those predicted by the weakly compressible liquid model (1%).

Flow formation in the weakly compressible fluid starts with a compression wave propagating from the front boundary to the outlet and separating stationary and moving fluid regions. This wave reaching the outlet reflects as rarefaction one and moves upwind accompanied by flow acceleration and finally gives rise to a new compression.

This repetitive process leading to the constant pressure gradient is manifested in the velocity variations on the graph shown in figure 5 (a black line). The amplitude of these oscillations decreases in the length of time. One can also note that the velocity increment due to rarefaction wave several times higher compared to that one in compression wave. The growth rate curve U/U_{axial} being independent of the pressure gradient Δp, as well as the sound speed c in the whole range of the calculation parameters (see figure 5) appears to be the most remarkable result. U and U_{axial} denote current step axial velocity and reference velocity according to (80). Due to the non-linear form of invariants transferred, this phenomenon can represent a class of self-similar solutions for the weakly compressible fluid flow in a plane channel.

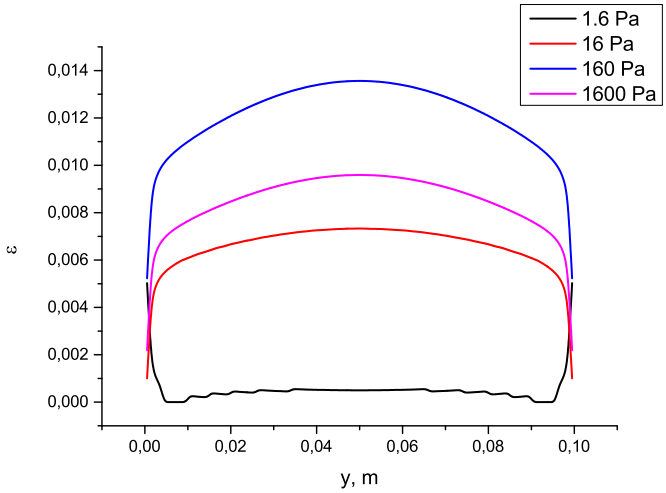

Figure 4. Relative error ϵ in a steady-state Poiseuille flow as a function of spanwise position at various pressure differentials.

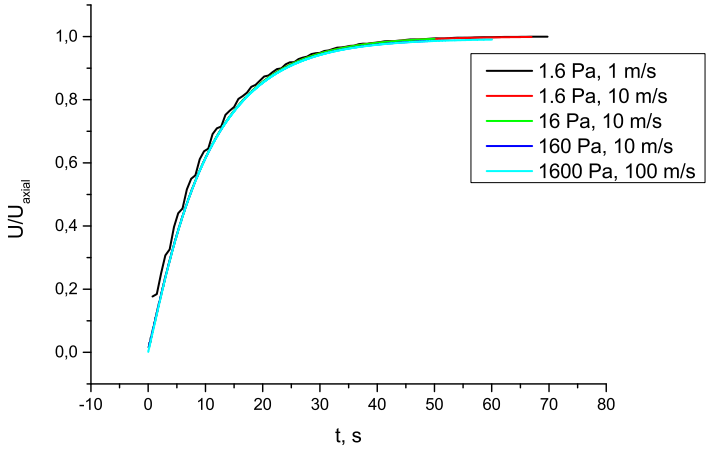

Figure 5. A set of axial velocity growth rate curves at various pressure drops and sound velocities. The axial velocity magnitude is normalized by the corresponding steady-state value U_{axial} calculated analytically.

One of the drawbacks of weakly compressible fluid model exactly noted in a peer review is a slow decrease of a residual norm

$$\frac{\delta U}{U_a} = \frac{|U - U_a|}{U_a}, \tag{82}$$

with iterations number growing determined as maximum relative difference between numerical velocity value and analytical one that is located at a flow axis, i.e. U_a corresponds to an axial velocity. This problem is of particular importance for pressure-driven flows (see figure 6). It should be noted that the optimum sound speed for calculation falls in a range $c = 50U_a$–$100U_a$,

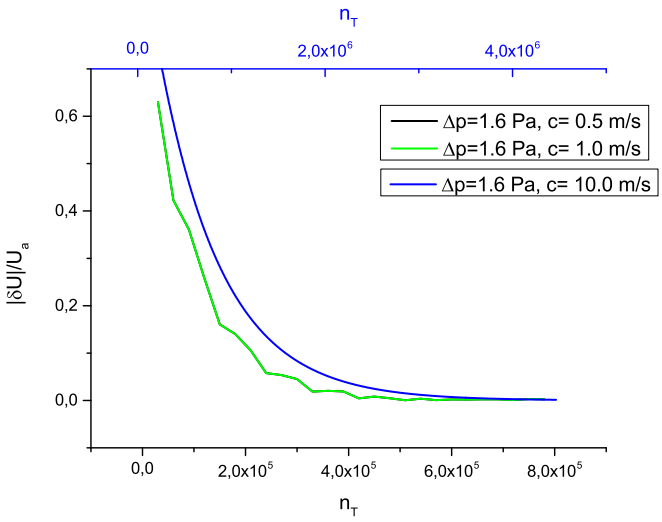

Figure 6. A residual norm as a function time steps number for various sound sound velocities. A blue-colored top axis corresponds to the case of $c = 10.0$ m/s.

if $c \approx 10U_a$, an excessive fluid acceleration occurs that consequently slows the convergence rate. Conversely, at $c \gg U_a$, the residual norm appears to be a logarithmic function of time steps number and solution time becomes unreasonably large.

4. Conclusion

The CABARET method represents a novel approach to solving fluid mechanics problems with dominating convective transport and can be successfully used for simulation of gasdynamic and incompressible fluid flows. The CABARET implementation for weakly compressible fluid flows proved to maintain all important advantages of general approach such as the absence of oscillations when calculating discontinuous flows, negligible dispersion and dissipation.

Testing of plane Poiseuille flow has shown that the results can be obtained with adequate precision, but not less than that predicted by the model of weakly compressible fluid (1%). An important feature of the considered pressure-driven flow is the self-similarity of velocity growth rate curves in terms of varying the pressure drop and the sound speed.

Acknowledgments

The work was supported by the Russian Science Foundation (project No. 14-50-00124).

References

[1] Goloviznin V M and Samarskii A A 1998 *Mat. Model.* **10** 101–116
[2] Goloviznin V M, Zaitsev M A, Karabasov S A and Korotkin I N 2012 *Novel Algorithms of Computational Hydrodynamics for Multicore Computing* (Moscow: University Press)
[3] Goloviznin V M, Hynes T P and Karabasov S A 2001 *Math. Modell. Anal.* **6** 210–220
[4] Vyaznikov K V, Tishkin V F and Favorskij A P 1989 *Mat. Model.* **1** 95–120
[5] Glotov V Yu and Goloviznin V M 2013 *Comput. Math. Math. Phys.* **53** 721–735
[6] Glotov V Yu and Goloviznin V M 2012 *Math. Model. Comput. Simul.* **4** 144–154
[7] Cherny G G 1988 *Gas Dynamics* (Moscow: Nauka)